Electronic transport in $Eu_{1-x}Ca_xB_6$

S. Paschen,* D. Pushin, M. Schlatter, P. Vonlanthen, and H. R. Ott
Laboratorium für Festkörperphysik, Eidgenössische Technische Hochschule–Hönggerberg, 8093 Zürich, Switzerland

D. P. Young and Z. Fisk
National High Magnetic Field Laboratory, Florida State University, 1800 East Paul Dirac Drive, Tallahassee, Florida 32306

(Received 7 July 1999; revised manuscript received 18 October 1999)

We have measured the electrical resistivity, the magnetoresistance, the Hall effect, and the magnetization in varying temperature ranges between 0.3 and 300 K on single crystals of EuB_6, CaB_6, and $Eu_{0.8}Ca_{0.2}B_6$. The ferromagnetic phase transition of EuB_6, marked by a sharp peak in the temperature dependence of the electrical resistivity $\rho(T)$ just below 16 K, is shown to be accompanied by a considerable increase of the effective charge carrier concentration n_{eff}. The overall features of the transport properties of $Eu_{0.8}Ca_{0.2}B_6$ are similar to those of EuB_6. A phase transition at 5.3 K has been established. However, the increase of n_{eff} across this phase transition by two orders of magnitude is much more pronounced than in pure EuB_6.

I. INTRODUCTION

It has been known for some time that the onset of magnetic order in EuB_6 is accompanied by a large reduction of the electrical resistivity.[1] More recently, the previously suggested ferromagnetic character of the ordered state has been confirmed by neutron-scattering measurements.[2] The same experiments also confirmed that the aligned magnetic moments are due to the localized $4f$ electrons of the Eu^{2+} ions and are of the expected magnitude of $7\mu_B$/Eu ion. In the paramagnetic state the temperature dependence of the electrical resistivity is of metallic character but the concentration of itinerant charge carriers is known to be rather small.[1,3–7] It is therefore not *a priori* clear whether the spontaneous alignment of the localized moments is simply due to the usual Ruderman-Kittel-Kasuya-Yosida interaction or whether also other coupling mechanisms might be of significance. A possible route to ferromagnetism in EuB_6 was very recently proposed from a mean-field treatment including the effect of the bond-charge Coulomb repulsion by Hirsch.[8] He argues that in EuB_6, and possibly also in other metallic systems, ferromagnetism is driven by a band broadening or equivalently an effective mass reduction, both occurring upon spin polarization. Hirsch takes the point of view that the giant shift of the plasma edge observed in optical reflectivity measurements on EuB_6 by Degiorgi *et al.*[9] is mainly due to an effective-mass variation. In this contribution, however, we show by temperature and magnetic-field dependent Hall-effect measurements that in EuB_6 a considerable change in the effective charge-carrier concentration occurs upon spin polarization. From these measurements and the data of Ref. 9 we give an estimate for the variation of the effective mass across the ferromagnetic phase transition.

A completely different type of ferromagnetism has recently been discovered in $Ca_{1-x}La_xB_6$.[10] Here the ferromagnetic polarization is thought to be a manifestation of a new ground state of the low-density ensemble of itinerant electrons, which is amazingly stable up to temperatures of the order of 1000 K. Therefore we have also investigated the electrical transport properties of CaB_6 and of $Eu_{0.8}Ca_{0.2}B_6$ and compare them with the results on EuB_6. As Ca and Eu are both divalent cations in the respective hexaborides, replacing Eu in EuB_6 by Ca should have no sizeable effect on the density of conduction electrons. Thus the charge-carrier concentrations in EuB_6, CaB_6, and $Eu_{0.8}Ca_{0.2}B_6$ are all expected to be similar. What is, however, drastically altered when replacing Eu in EuB_6 by Ca is the regular array of $4f$-electron moments.

II. SAMPLES AND EXPERIMENTAL METHODS

The single-crystalline EuB_6, CaB_6, and $Eu_{0.8}Ca_{0.2}B_6$ samples were prepared by solution growth from Al flux, using the appropriate amounts of the pure elements. Flux-grown SrB_6 samples have been shown to be of high structural and chemical quality.[11] In addition to EuB_6, containing the isotopes ^{10}B and ^{11}B in the ratio given by their natural abundance of approximately 1:4, we have also investigated $Eu^{10}B_6$ and $Eu^{11}B_6$ samples containing only the isotopes ^{10}B and ^{11}B, respectively. By this approach we hoped to disentangle some of the complicated features observed in conventional EuB_6 samples with the natural mixture of B isopopes. A non-negligible influence might be expected if polaronic effects are important in the low-temperature behavior of EuB_6.

The electrical resistivity, the magnetoresistance, and the Hall effect were measured by a standard low-frequency ac technique in varying temperature ranges between 0.3 and 300 K and in magnetic fields of up to 70 kOe. The magnetoresistance was measured in a transverse configuration, i.e., the magnetic field $\vec{H}$ was applied perpendicular to the electrical current $\vec{I}$. For the Hall-effect measurements a standard setup with the two Hall voltage contacts perpendicular to $\vec{I}$ and to $\vec{H}$ was used. In order to eliminate the misalignement voltage, the sample was, at each field setting, first measured in an upright position, then turned by 180°, and subsequently measured in a downward position. At each temperature a sweep of the magnetic field was performed, stabilizing the temperature with a capacitance thermometer. For EuB_6 and $Eu_{0.8}Ca_{0.2}B_6$ the electrical leads were contacted to the sample

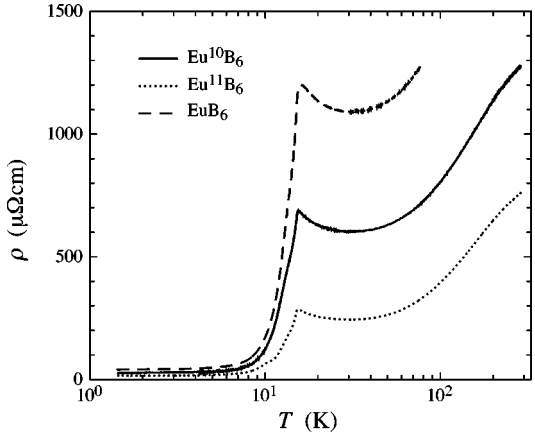

FIG. 1. Electrical resistivity ρ vs temperature T for EuB_6 samples 1 ($Eu^{10}B_6$), 2 ($Eu^{11}B_6$), and 3 (EuB_6).

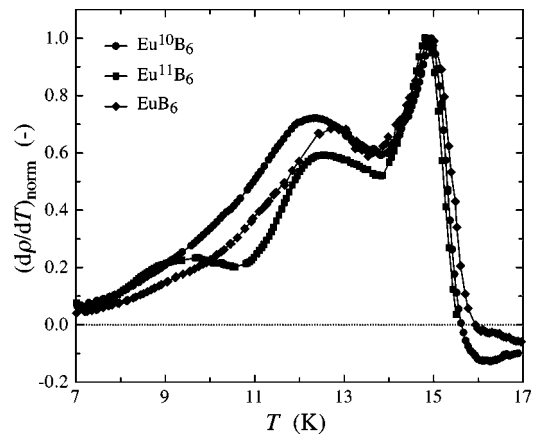

FIG. 2. Numerically calculated temperature derivative of the electrical resistivity $\partial\rho/\partial T$ normalized to its maximum value as a function of temperature T for the EuB_6 samples 1 ($Eu^{10}B_6$), 2 ($Eu^{11}B_6$), and 3 (EuB_6). The solid lines are to guide the eye.

with silver epoxy, for CaB_6 spring contacts were used. The magnetic measurements were performed in a commercial superconducting quantum interference device magnetometer in the temperature range 1.9–300 K.

III. EXPERIMENTAL RESULTS AND ANALYSIS

Our results for the temperature dependence of the electrical resistivity $\rho(T)$ of the EuB_6 samples are, in magnitude and shape, very similar to those that have been published previously[1,3–7,12,13] and are displayed in Fig. 1. In the following we refer to the samples $Eu^{10}B_6$, $Eu^{11}B_6$, and EuB_6 as sample 1, 2, and 3, respectively. It may be seen that the general features of $\rho(T)$ are the same for all three samples but the absolute magnitudes of the resistivities are quite different. We have no obvious explanation for the latter fact. Between room temperature and approximately 30 K, ρ decreases as T decreases, a sign of common metallic behavior. At lower temperatures $\rho(T)$ increases, passes through a cusplike maximum just below 16 K, and subsequently falls off steeply to the lowest measured temperatures. Below 3 K, $\rho(T)$ of all three samples is well described by $\rho=\rho_0+AT^2$ with $\rho_0=26.8$, 15.1, and 40.3 $\mu\Omega$ cm and $A=0.28$, 0.08, and 0.24 $\mu\Omega\,\mathrm{cm\,K^{-2}}$ for sample 1, 2, and 3, respectively. The residual resistivity ρ_0 being the highest for the mixed-isotopes sample may be related with enhanced disorder due to the presence of both ^{10}B and ^{11}B.

In Fig. 2 we carefully analyze $\rho(T)$ of all three EuB_6 samples in the temperature range between 7 and 17 K, by plotting the numerically calculated derivative $\partial\rho/\partial T$ as a function of temperature. The passage through zero of $\partial\rho/\partial T$, corresponding to the maximum of $\rho(T)$, is followed by two (samples 1 and 3) or even three (sample 2) maxima. The temperatures at which $\partial\rho/\partial T$ passes through zero are 15.6, 15.5, and 15.9 K for sample 1, 2, and 3, respectively. A comparison with our temperature-dependent magnetic susceptibility measurements indicates that these temperatures mark the onset of ferromagnetic order and thus have to be identified with the Curie temperature T_C. The temperature of the first maximum of $\partial\rho/\partial T$ which we call T_1 is, within experimental uncertainty, the same for all three samples (14.9 K for samples 1 and 3, 14.8 K for sample 2), but the temperature of the second maximum called T_2 is less well defined (12.4 K for sample 1, 12.5 K for sample 2, 12.8 K for sample 3). The third maximum at $T_3=9.6$ K is observed only for sample 2. Measurements of the specific heat[9,13] revealed the occurence of two consecutive phase transitions in EuB_6. Our $\rho(T)$ data show that the phase transition is even more complicated and that the details at temperatures below T_C may be quite sample dependent. The Curie temperature T_C is, within 0.4 K, the same for all our samples. From these data we have no unambiguous evidence for a B isotope effect on the ferromagnetic transition in EuB_6.

We now turn to the electrical resistivity data of CaB_6 and $Eu_{0.8}Ca_{0.2}B_6$which are shown in Figs. 3 and 4, respectively. It may be seen that ρ of CaB_6 varies much less with temperature than ρ of EuB_6. Below room temperature ρ of CaB_6 decreases, reaching a minimum at 116 K. After a subsequent increase it passes through a maximum at 53 K and again through a further minimum at 10.8 K. Finally it increases smoothly with decreasing temperature to 1.5 K. More pronounced features of $\rho(T)$ are recognized for $Eu_{0.8}Ca_{0.2}B_6$. The dominating sharp maximum at 5.3 K is preceded by a shallow maximum at 208 K and a shallow minimum at 34 K. The subsequent decrease of $\rho(T)$ is intercepted by a minimum at 2.5 K below which $\rho(T)$ increases towards the lowest measured temperatures. For comparison, Fig. 5 gives an overview of the temperature dependences of the electrical

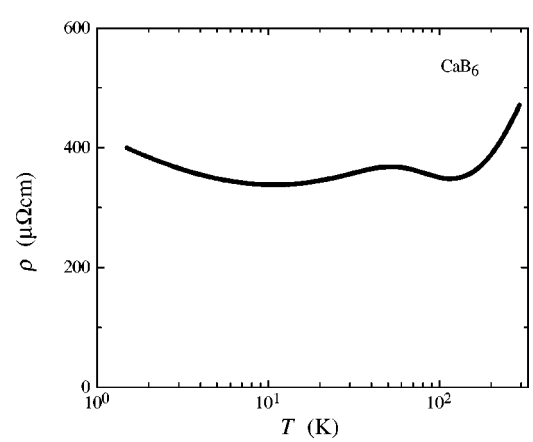

FIG. 3. Electrical resistivity ρ vs temperature T for CaB_6.

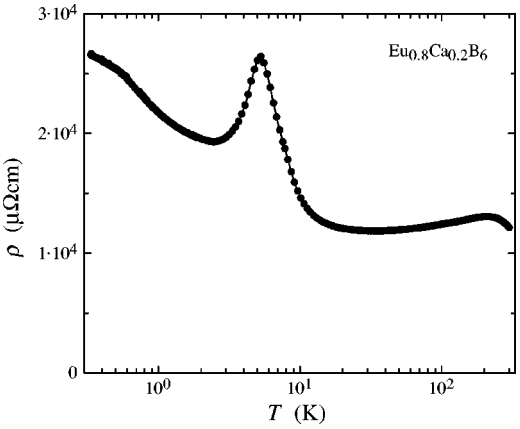

FIG. 4. Electrical resistivity ρ vs temperature T for $Eu_{0.8}Ca_{0.2}B_6$. The solid line is to guide the eye.

resistivities $\rho(T)$, normalized to the room-temperature value, of EuB_6 sample 1, CaB_6, and $Eu_{0.8}Ca_{0.2}B_6$.

In Fig. 6 we replot the temperature dependence of the electrical resistivity of the EuB_6 sample 1 [Fig. 6(a)], and of $Eu_{0.8}Ca_{0.2}B_6$ [Fig. 6(b)], together with the magnetic susceptibilities χ of both samples. Just as for EuB_6 the cusplike feature of $\rho(T)$ of $Eu_{0.8}Ca_{0.2}B_6$ at 5.3 K is accompanied by a sharp increase of χ with decreasing temperature. This is a clear indication that also $Eu_{0.8}Ca_{0.2}B_6$ orders ferromagnetically, at a substantially reduced Curie temperature, however. The saturation magnetization at 1.9 K is approximately 5 μ_B per Eu ion, distinctly reduced if compared to approximately 7μ_B per Eu ion for EuB_6.

In the following we present our Hall effect measurements. For pure EuB_6, low-temperature and low-field Hall-effect data are available in the literature.[5,7] The effective charge-carrier concentration at 4.2 K that we have derived from our Hall constant at 1 T agrees, within factors of 0.7 and 1.1, with those derived from the low-field Hall constants of Refs. 5 and 7, respectively. The field dependence of the Hall resistivity of EuB_6 in magnetic fields up to 70 kOe, to be presented below, has, to our knowledge, not yet been published.

The Hall effect shows the most spectacular features for $Eu_{0.8}Ca_{0.2}B_6$and we shall present these data first. In Fig. 7

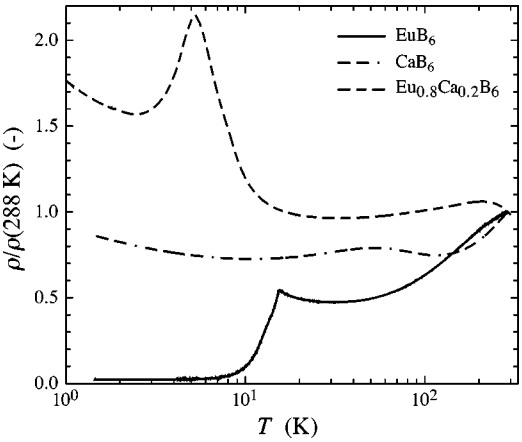

FIG. 5. Electrical resistivity ρ normalized to the value at 288 K vs temperature T for EuB_6 sample 1 ($Eu^{10}B_6$) and for CaB_6 and $Eu_{0.8}Ca_{0.2}B_6$.

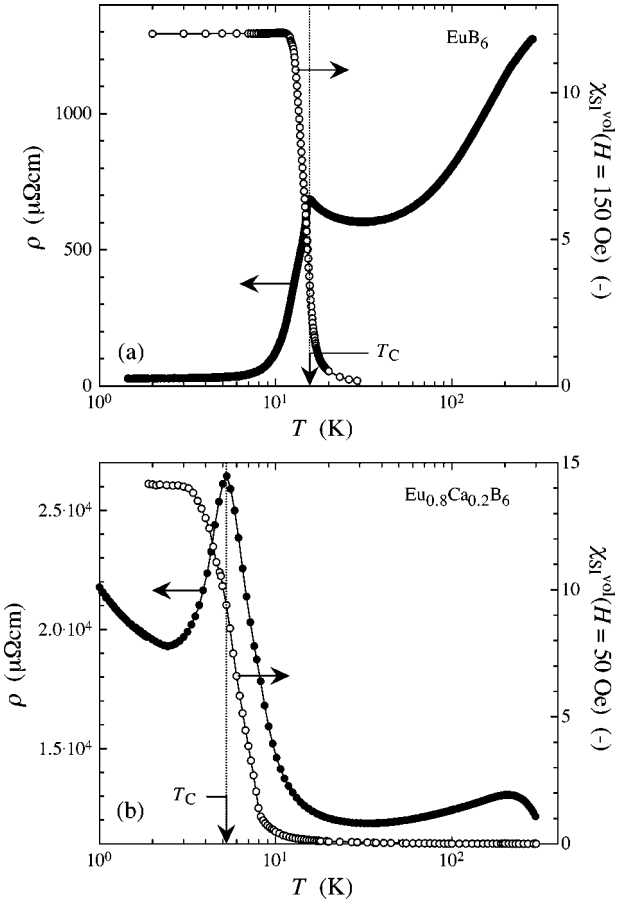

FIG. 6. Electrical resistivity ρ and magnetic susceptibility χ in SI units vs temperature T for EuB_6 sample 1 ($Eu^{10}B_6$) in (a) and for $Eu_{0.8}Ca_{0.2}B_6$in (b). The Curie temperatures T_C are 15.6 and 5.3 K for EuB_6 and $Eu_{0.8}Ca_{0.2}B_6$, respectively. The solid lines are to guide the eye.

some representative data of the Hall resistivity $\rho_H = V_H d/I$ of $Eu_{0.8}Ca_{0.2}B_6$, measured at fixed temperatures between 2 and 290 K, is plotted as a function of the magnetic induction $B = \mu_0 H$, where H is the external magnetic field and μ_0 the permeability of free space. V_H is the Hall voltage, d the

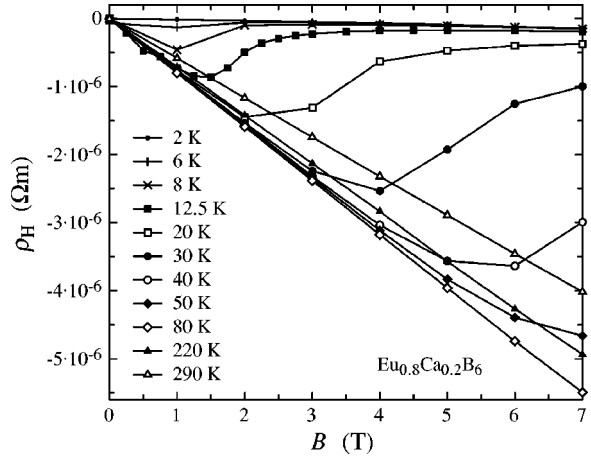

FIG. 7. Hall resistivity ρ_H of $Eu_{0.8}Ca_{0.2}B_6$, measured at fixed temperatures between 2 and 290 K, as a function of the magnetic induction B. The solid lines are to guide the eye.

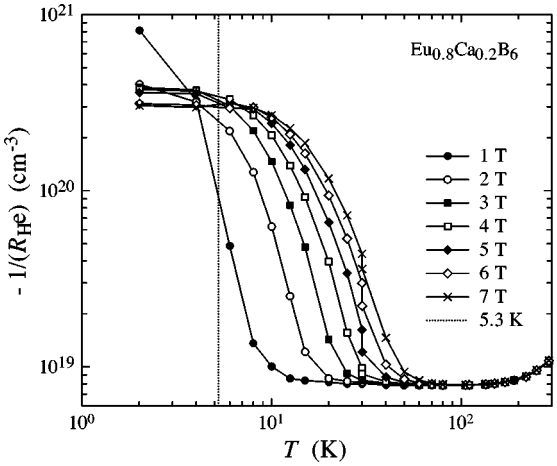

FIG. 8. Effective charge-carrier concentration $-1/(R_He)$ of $Eu_{0.8}Ca_{0.2}B_6$ at different values of B between 1 and 7 T as a function of temperature T. The Hall coefficient R_H was calculated at each B value by $R_H(B)=\rho_H(B)/B$. The dotted line indicates the Curie temperature determined from the position of the maximum of $\rho(T)$. The solid lines are to guide the eye.

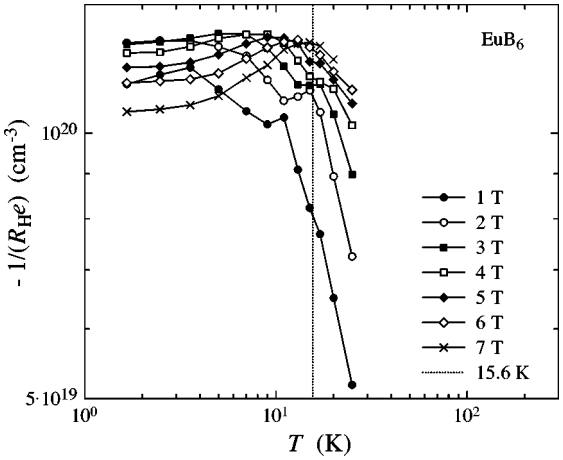

FIG. 9. Effective charge-carrier concentration $-1/(R_He)$ of EuB_6 sample 1 ($Eu^{10}B_6$) at different values of B between 1 and 7 T as a function of temperature T. The Hall coefficient R_H was calculated at each B value by $R_H(B)=\rho_H(B)/B$. The dotted line indicates the Curie temperature determined from the position of the maximum of $\rho(T)$. The solid lines are to guide the eye.

sample thickness, and I the applied current. Between 290 and approximately 80 K, ρ_H is a linear function of B up to $B=7$ T. At lower temperatures ρ_H deviates from the linear dependence at inductions B that decrease with decreasing temperature. At 2 K, an almost linear dependence with a slope whose absolute value is much smaller than at high temperatures is recovered. Attempts to fit the highly nonlinear $\rho_H(B)$ curves in the range between 2 and 80 K by either a two band model or by considering the anomalous Hall effect via our magnetization measurements on $Eu_{0.8}Ca_{0.2}B_6$ in magnetic fields of up to 55 kOe, were not successful. Neither of these considerations lead to an even qualitative agreement between calculations and experiment. Therefore we suggest that the nonlinear $\rho_H(B)$ behavior results from a magnetic-field-induced transition between a charge-carrier-poor state at high temperatures [linear $\rho_H(B)$ dependence with a large absolute value of the slope] to a charge-carrier-rich state [linear $\rho_H(B)$ dependence with a small absolute value of the slope] at low temperatures. The temperature at which this transition occurs increases with increasing applied magnetic field. This is more clearly revealed by Fig. 8, where we plot $-1/(R_He)$ at different values of B between 1 and 7 T as a function of temperature. The Hall coefficient R_H was calculated at each B value by $R_H(B)=\rho_H(B)/B$. The ratio $-1/(R_He)$ may be interpreted as an effective charge-carrier concentration. R_H is negative at all fields and at all temperatures which implies that the charge carriers are predominantly electronlike. Above 80 K all curves in Fig. 8 fall on top of each other, reflecting the linear variation of $\rho_H(B)$. At lower temperatures all $-1/(R_He)$ curves reveal a steep increase over more than one order of magnitude. The temperatures fixed by the largest slope of this increase range between approximately 30 K for the curve at 7 T and approximately 5 K for the curve at 1 T. The effective electron concentration is approximately 8×10^{18} cm^{-3} above the transition and between 3 and 8×10^{20} cm^{-3} below the transition. The curve at 1 T reflects most closely the intrinsic (zero-field) behavior of $Eu_{0.8}Ca_{0.2}B_6$. The fact that the temperature of the maximum negative slope of the 1-T curve coincides with the Curie temperature of $Eu_{0.8}Ca_{0.2}B_6$ (dotted line in Fig. 8) indicates that the drastic increase of the charge-carrier concentration is directly related to the ferromagnetic phase transition.

The Hall effect of pure EuB_6 is qualitatively similar to the one of $Eu_{0.8}Ca_{0.2}B_6$, but the features described above are somewhat less pronounced in the case of EuB_6. In Fig. 9 we plot $-1/(R_He)$, obtained as explained above, at fixed fields between 1 and 7 T as a function of temperature. The analogy between the curves of $Eu_{0.8}Ca_{0.2}B_6$ and EuB_6 is not really obvious at first sight because the investigated temperature range with respect to the Curie temperature is much less extended for EuB_6, for which measurements only below 25 K have been made. Only the low-temperature tail of the field-induced phase transition from a state with low charge-carrier concentration at high temperatures to a state with high charge-carrier concentration at low temperatures is experimentally established. However, we speculate that at temperatures well above the Curie temperature of EuB_6, all curves of Fig. 9 will merge and assume a value somewhat smaller than 5×10^{19} cm^{-3}. Well below T_C, the ratio $-1/(R_He)$ tends to decrease again, at least for external fields exceeding 3 T. For $B=7$ T the effective charge-carrier concentration assumes a maximum at approximately 14 K and clearly decreases towards lower temperatures. In smaller fields the position of this maximum shifts to lower temperatures and the decrease is less pronounced.

The Hall-effect data of CaB_6 is much easier to analyze. The Hall resistivity $\rho_H(B)$ varies approximately linearly with B in the entire investigated temperature range between 1.9 and 280 K. The slope of all $\rho_H(B)$ curves is negative, implying predominant electron-type conduction. The corresponding effective charge-carrier concentration reaches values between 1.8 and 2.4×10^{19} cm^{-3}. At 53 K, the temperature where $\rho(T)$ reaches a maximum, the electron concentration increases slightly. This feature is reminescent of those in $\rho(T)$ and $n(T)$ at the ferromagnetic phase transition in EuB_6 and $Eu_{0.8}Ca_{0.2}B_6$.

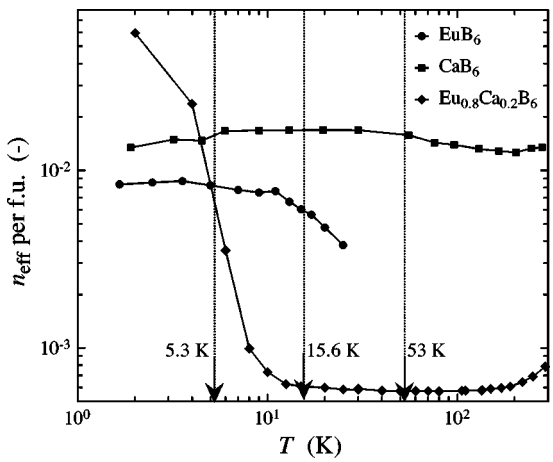

FIG. 10. Effective charge-carrier concentration per formula unit n_{eff} determined from the Hall coefficient at 1 T of EuB_6 sample 1 ($Eu^{10}B_6$), CaB_6, and $Eu_{0.8}Ca_{0.2}B_6$as a function of temperature T. The dotted lines indicate the positions where the respective $\rho(T)$ curves assume a maximum. The solid lines are to guide the eye.

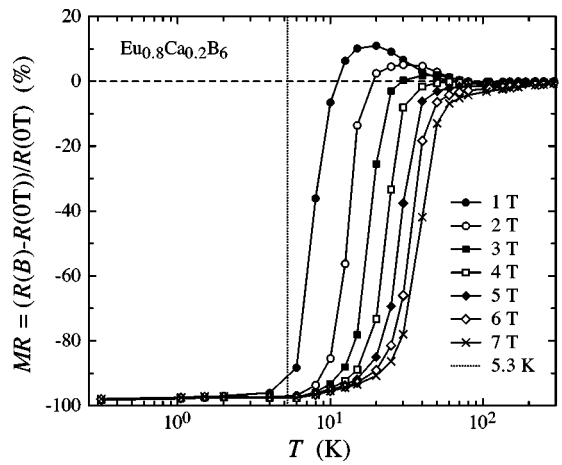

FIG. 12. Magnetoresistance $MR=[R(B)-R(0)]/R(B)$ of $Eu_{0.8}Ca_{0.2}B_6$at different B values between 1 and 7 T as a function of temperature T. The dotted line indicates the Curie temperature determined from the position of the maximum of $\rho(T)$. The solid lines are to guide the eye.

An overview over the low-field Hall-effect data of all three investigated samples, EuB_6, CaB_6, and $Eu_{0.8}Ca_{0.2}B_6$, is given in Fig. 10 where we plot the effective charge-carrier concentration $n_{\mathrm{eff}}=-1/[R_{\mathrm{H}}(B=1\ \mathrm{T})e]$ per formula unit as a function of temperature at 1 T. For the lattice constants we used 4.1852 Å for EuB_6,[13] 4.146 Å for CaB_6,[14] and an interpolation between both values for $Eu_{0.8}Ca_{0.2}B_6$. For $Eu_{0.8}Ca_{0.2}B_6$ n_{eff} increases most dramatically across the magnetic transition at 5.3 K (by two orders of magnitude) with decreasing temperature. For EuB_6 n_{eff} increases by at least a factor of 2.3 and the transition temperature is considerably higher. For CaB_6 a slight increase of n_{eff} may be identified between 200 and 30 K. The effective charge-carrier concentration is, with less than 0.1 electron per formula unit at all temperatures, rather low for all three materials. For $Eu_{0.8}Ca_{0.2}B_6$ we find, with less than 6×10^{-4} charge carriers per formula unit, an exceedingly low effective carrier concentration at high temperatures.

Finally, we present our magnetoresistance data. In Fig. 11 we plot the magnetoresistance $\mathrm{MR}=[R(B)-R(0)]/R(B)$ of EuB_6 sample 1 ($Eu^{10}B_6$) at different B values between 1 and 7 T as a function of temperature T. The solid lines are to guide the eye.

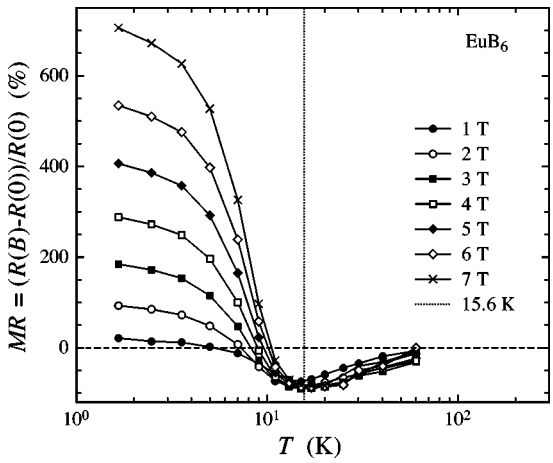

FIG. 11. Magnetoresistance $MR=[R(B)-R(0)]/R(B)$ of EuB_6 sample 1 ($Eu^{10}B_6$) at different B values between 1 and 7 T as a function of temperature T. The solid lines are to guide the eye.

EuB_6 sample 1 at different B values between 1 and 7 T as a function of temperature. As previously reported,[5,7,13] the high-temperature MR is negative, increasing in absolute value with decreasing temperature. The maximum negative MR of approximately 100% is reached at the Curie temperature of EuB_6. At lower temperatures the absolute value of the MR decreases, passes through zero, and reaches positive values as high as 700% at 7 T and 1.7 K.

Above T_{C}, the magnetoresistances of EuB_6 and $Eu_{0.8}Ca_{0.2}B_6$ are qualitatively similar. As is shown in Fig. 12, above T_{C} the MR of $Eu_{0.8}Ca_{0.2}B_6$ is, except for small positive values at small fields, negative and increases in absolute value with decreasing temperature. At T_{C} a maximum absolute value of almost 100% is reached, just as for EuB_6. However, in contrast to the MR of EuB_6, the MR of $Eu_{0.8}Ca_{0.2}B_6$ remains negative at temperatures well below T_{C}.

IV. DISCUSSION

The results of recent band-structure calculations by Massida *et al.*[15] suggest that the cubic hexaborides CaB_6 and EuB_6 are semimetals, with a small band overlap at the X point of the Brillouin zone. In a perfect semimetal the concentration of electrons in the conduction band is the same as the concentration of holes in the valence band. The Hall coefficient of such a system is only nonzero if the electron and hole mobilities are not the same. The fact that we find a negative Hall coefficient for all samples in the entire temperature range indicates that the electrons are more mobile than the holes. This is in agreement with the band structure of Ref. 15 where, at the X point, the effective mass of the charge carriers in the conduction band of both CaB_6 and EuB_6 is smaller than the one of the holes in the valence band. The effective charge-carrier concentration n_{eff} discussed in the previous section is, in a perfect semimetal, related to the real electron (or hole) concentration n by $n_{\mathrm{eff}}=n(\mu_{\mathrm{p}}+\mu_{\mathrm{n}})/(\mu_{\mathrm{p}}-\mu_{\mathrm{n}})$, where μ_{p} and μ_{n} are the hole and electron mobility, respectively. Thus the real electron concentrations n in EuB_6, CaB_6, and $Eu_{0.8}Ca_{0.2}B_6$ may even be smaller than

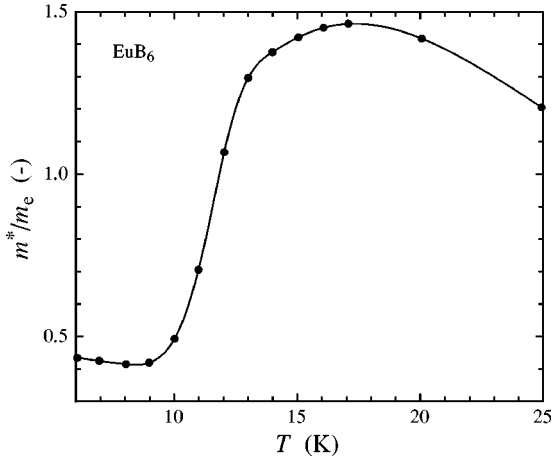

FIG. 13. Temperature dependence of the effective mass ratio m^*/m_e (m_e = mass of free electron) of EuB_6 sample 1 (Eu $^{10}B_6$) obtained by combining the effective charge-carrier concentration of Fig. 10 with the temperature dependence of the plasma frequency given by Degiorgi *et al.* (Ref. 9). The dots mark the data points and the solid curve is obtained by a smooth interpolation between them.

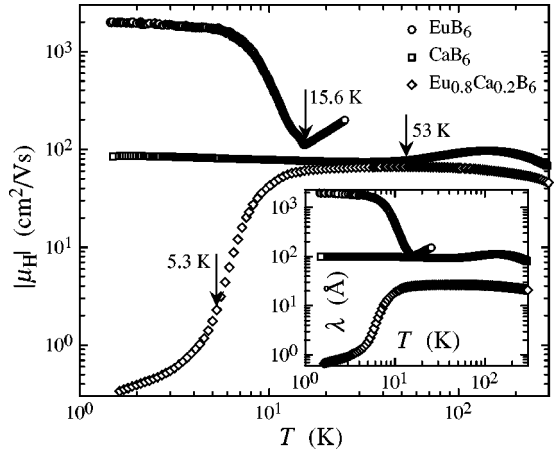

FIG. 14. Absolute value of the Hall mobility $|\mu_H|$ of EuB_6 sample 1 ($Eu^{10}B_6$), CaB_6, and $Eu_{0.8}Ca_{0.2}B_6$vs temperature T. The inset shows the temperature dependence of the ''Hall'' mean free path λ of the same three samples obtained as explained in the text.

the effective charge-carrier concentrations n_{eff} given in Fig. 10. Likewise, it cannot be excluded that μ_p and μ_n have a different temperature dependence which would affect the way in which n is changed across the phase transition. However, this effect shall be neglected in the following estimate.

As mentioned in the introduction measurements of the optical reflectivity of single-crystalline EuB_6 (same sample as sample 3 of this study) revealed a large shift of the plasma edge below T_C.[9] The unscreened plasma frequency ω_p was shown to increase from approximately 2060 cm^{-1} at 20 K to approximately 4890 cm^{-1} at 6 K. As pointed out by Degiorgi *et al.*[9] this shift suggests an increase of the itinerant charge-carrier concentration, a reduction of their effective mass, or a combination of the two. Combining the $\omega_p(T)$ data of Ref. 9 with our low-field Hall-effect data of EuB_6 (cf. Fig. 10) using the relation $\omega_p=(ne^2/\epsilon_0 m^*)^{1/2}$ with $n=-1/[R_H(B=1\ T)e]$ we can estimate the temperature dependence of the effective mass m^*. ϵ_0 is the permittivity of free space. In Fig. 13 we plot the ratio m^*/m_e, where m_e is the mass of a free electron, between 6 and 25 K, the temperature range where both ω_p and $R_H(B=1\ T)$ have been measured. With decreasing temperature m^*/m_e first slightly increases and, between 17 and 9 K, drops by a factor of 3.5, a substantial reduction. Thus, in addition to an increase of the charge-carrier concentration, the effective mass of the charge carriers is reduced in the course of the ferromagnetic phase transition. As mentioned in the Introduction, Hirsch proposed a model for EuB_6 in which the entire shift of ω_p can be explained by a shift of the effective mass.[8] Our results may thus serve to refine this model.

Very recently, Aronson *et al.*[16] reported on results of their Shubnikov–de Haas and de Haas–van Alphen measurements on a EuB_6 single crystal. From the smooth temperature dependences below 25 K of four fundamental frequencies, extracted from measurements at fields between 5 and 30 T, they conclude that the Fermi surface of EuB_6 is essentially unaffected by the onset of magnetism. Our Hall-effect measurements, however, show that in the temperature range around T_C the Fermi surface is very sensitive to magnetic fields. An appreciable decrease of the effective charge-carrier concentration across the (zero-field) Curie temperature T_C is deduced from the low-field Hall constant only. Higher fields shift the decrease of the effective charge-carrier concentration to higher temperatures. In the case of $Eu_{0.8}Ca_{0.2}B_6$, the temperature fixed by the largest slope of this decrease is shifted from 5 K at 1 T to 30 K at 7 T. A similar sensitivity is anticipated for EuB_6 (cf. Fig. 9). Therefore we believe that the above-mentioned high-field measurements[16] cannot rule out an appreciable modification to the Fermi-surface dimensions with the onset of ferromagnetism.

Combining the resistivity and the Hall-effect data we may calculate both the low-field Hall mobility $\mu_H=R_H(B=1\ T)/\rho$ and the ''Hall'' mean free path $\lambda=\hbar(3\pi^2/e^4)^{1/3}[R_H(B=1\ T)]^{2/3}/\rho$, which we plot in Fig. 14 and in its inset, respectively, as a function of temperature for EuB_6 sample 1, CaB_6, and $Eu_{0.8}Ca_{0.2}B_6$. The absolute value of the Hall mobility $|\mu_H|$ of EuB_6 has a sharp minimum at the Curie temperature of 15.6 K. Below T_C, $|\mu_H|$ of EuB_6 increases steeply by an order of magnitude and reaches values as high as 2000 $cm^2/V\,s$ at 1.5 K. For $Eu_{0.8}Ca_{0.2}B_6$ $|\mu_H|$ passes over a broad maximum centered at 50 K from where it falls by two orders of magnitude with decreasing temperature to 0.3 $cm^2/V\,s$ at 1.6 K. Unlike in the case of EuB_6, $|\mu_H|$ of $Eu_{0.8}Ca_{0.2}B_6$ does not increase below T_C but instead continues to drop. For CaB_6 $|\mu_H|$ varies much less with temperature. It passes over a maximum at 140 K and through a shallow minimum at 30 K. With absolute values of the order of 100 $cm^2/V\,s$ in the entire temperature range the Hall mobility of CaB_6 lies inbetween the ones of EuB_6 and $Eu_{0.8}Ca_{0.2}B_6$. For all three samples the temperature dependence of the ''Hall'' mean free path λ resembles that of $|\mu_H|$. The ''Hall'' mean free path of $Eu_{0.8}Ca_{0.2}B_6$ above T_C, being considerably shorter than the ones of EuB_6 and CaB_6, might be due to the disorder introduced into the system by Ca doping. It is somewhat surprising that λ of EuB_6 below T_C is much longer than λ of CaB_6. It should be kept in mind, however, that the Hall mobility and the ''Hall'' mean free path are only effective parameters in a fictitious one band model. In a perfect semimetal the Hall mobility is related to

the electron and hole mobilities by $\mu_H = \mu_p - \mu_n$, i.e., a small absolute value of the Hall mobility (and a short ''Hall'' mean free path) can also be due to μ_p and μ_n being coincidentally very similar in magnitude. In view of this likely complication we refrain from interpreting the overall features of $\mu_H(T)$ in detail at this time. Nevertheless, the increase of $|\mu_H|$ below T_C of EuB_6 is, in part, due to the decrease of the effective mass (cf. Fig. 13) but, in addition, there has to be a sizeable increase of the effective scattering time $\tau = m\mu/e$. Evidence for this has also been obtained from an analysis of the optical conductivity data presented in Ref. 9. This indicates that there must be a significant change in the scattering mechanism for itinerant charge carriers in EuB_6 induced by the phase transition.

V. CONCLUSIONS

We have shown that the ferromagnetic phase transition of EuB_6 at approximately 16 K is accompanied by a considerable increase of the effective charge-carrier concentration. Part of the giant shift of the plasma frequency deduced from optical reflectivity measurements[9] is thus due to an increase of the charge-carrier concentration upon spin polarization. In addition, both the effective mass and the effective scattering rate have been shown to be reduced upon spin polarization. Thus the ferromagnetic phase transition of EuB_6 has an appreciable effect on all three fundamental parameters (carrier concentration, mass, and scattering rate) and a serious comparison with any theoretical model cannot be made without disentangling these effects.

In $Eu_{0.8}Ca_{0.2}B_6$we have identified a ferromagnetic phase transition at 5.3 K, accompanied by an increase of the effective charge-carrier concentration by as much as two orders of magnitude. The carrier concentration at temperatures above the phase transition is, with less than 6×10^{-4} per formula unit, extremely low for a metallic system. In particular, it does not lie inbetween the carrier concentrations of EuB_6 and CaB_6. Thus it appears to be extremely interesting to further investigate $Eu_{1-x}Ca_xB_6$ samples and systematically follow the evolution of the Curie temperature and the charge carrier concentration upon Ca doping of EuB_6.

ACKNOWLEDGMENTS

We thank H. Thomas for technical assistance. This work was financially supported by the Schweizerische Nationalfonds zur Förderung der wissenschaftlichen Forschung.

*Present address: MPI for Chemical Physics of Solids, Nöthnitzer Str. 48, 01187 Dresden, Germany.

[1] Z. Fisk, D. C. Johnston, B. Cornut, S. von Molnar, S. Oseroff, and R. Calvo, J. Appl. Phys. **50**, 1911 (1979).
[2] W. Henggeler, H. R. Ott, D. P. Young, and Z. Fisk, Solid State Commun. **108**, 929 (1998).
[3] Y. Isikawa, M. M. Bajaj, M. Kasaya, T. Tanaka, and E. Bannai, Solid State Commun. **22**, 573 (1977).
[4] S. Oseroff, R. Calvo, J. Stankiewicz, Z. Fisk, and D. C. Johnston, Phys. Status Solidi B **94**, K133 (1979).
[5] C. N. Guy, S. von Molnar, J. Etourneau, and Z. Fisk, Solid State Commun. **33**, 1055 (1980).
[6] J. M. Tarascon, J. Etourneau, P. Dordor, P. Hagenmüller, M. Kasaya, and J. M. D. Coey, J. Appl. Phys. **51**, 574 (1980).
[7] G. Weill, I. A. Smirnov, and V. N. Gurin, J. Phys. (Paris), Colloq. **41**, C5-185 (1980).
[8] J. E. Hirsch, Phys. Rev. B **59**, 1 (1999).
[9] L. Degiorgi, E. Felder, H. R. Ott, J. L. Sarrao, and Z. Fisk, Phys. Rev. Lett. **79**, 5134 (1997).
[10] D. P. Young, D. Hall, M. E. Torelli, Z. Fisk, J. L. Sarrao, J. D. Thompson, H. R. Ott, S. B. Oseroff, R. G. Goodrich, and R. Zysler, Nature (London) **397**, 412 (1999).
[11] H. R. Ott, M. Chernikov, E. Felder, L. Degiorgi, E. G. Moshopoulou, J. L. Sarrao, and Z. Fisk, Z. Phys. B: Condens. Matter **102**, 337 (1997).
[12] J. C. Cooley, M. C. Aronson, J. L. Sarrao, and Z. Fisk, Phys. Rev. B **56**, 14 541 (1997).
[13] S. Süllow, I. Prasad, M. C. Aronson, J. L. Sarrao, Z. Fisk, D. Hristova, A. H. Lacerda, M. F. Hundley, A. Vigliante, and D. Gibbs, Phys. Rev. B **57**, 5860 (1998).
[14] R. Naslain, J. Etourneau, and P. Hagenmüller, in *Boron and Refractory Borides*, edited by V. I. Matkovich (Springer, Berlin, 1977), p. 262.
[15] S. Massidda, A. Continenza, T. M. de Pascale, and R. Monnier, Z. Phys. B: Condens. Matter **102**, 83 (1997).
[16] M. C. Aronson, J. L. Sarrao, Z. Fisk, M. Whitton, and B. L. Brandt, Phys. Rev. B **59**, 4720 (1999).